Inorganic Chemistry
Article

Inorg. Chem. **2010**, *49*, 3991–4001 **3991**
DOI: 10.1021/ic901925w

Rodlike Fluorescent π-Conjugated 3,3′-Bipyridazine Ligand: Optical, Electronic, and Complexation Properties

Frédéric Lincker,[†] David Kreher,[†] André-Jean Attias,*[,†] Jaekwon Do,[‡] Eunkyoung Kim,[‡] Philippe Hapiot,[§] Noëlla Lemaître,[∥] Bernard Geffroy,[⊥] Gilles Ulrich,[⊗] and Raymond Ziessel[⊗]

[†]*Université Pierre et Marie Curie - UMR CNRS 7610 - Laboratoire de Chimie des Polymères 4, place Jussieu - Case Courrier 185 F 75252 Paris CEDEX 05, France,* [‡]*Department of Chemical and Biomolecular Engineering, Yonsei University, 262 Seongsanno, Seodaemun-gu, Seoul 120-749, Korea,* [§]*Université de Rennes 1, Sciences Chimiques de Rennes, CNRS UMR 6226 Campus de Beaulieu F 35042 Rennes CEDEX, France,* [∥]*CEA INES − DRT/LITEN/DTS/LCP Savoie Technolac, 50 av. du Lac Léman, BP332 F 73377 Le Bourget du Lac CEDEX, France,* [⊥]*CEA-LITEN, LPICM, Ecole Polytechnique F 91128 Palaiseau, France, and* [⊗]*Laboratoire de Chimie Organique et Spectroscopies Avancées, CNRS, ECPM, UdS 25 rue Becquerel F 67087 Strasbourg CEDEX, France*

Received September 30, 2009

We report on the design and synthesis of a new quadrupolar π-conjugated 3,3′-bipyridazine D-A-D ligand. Its electronic and optical properties were investigated. Besides high fluorescence and pronounced solvatochromism, it exhibits an inherent electroactivity exploited to build an organic green light emitting device. Moreover, the ability of this ligand to complex metallic centers (Cu^{I}, Ni^{II}, Pt^{II}, and Ir^{III}) was also investigated to access different geometries and to tune their electronic and optical properties. These preliminary results open up the synthesis of heavy-metal complexes to obtain phosphorescent emitters.

Introduction

Throughout the past few decades, the development of new ligands and related coordination compounds has been an increasing field of research because of their potential applications ranging from self-assembly and supramolecular chemistry,[1] to solar energy conversion and storage,[2,3] and more recently to phosphorescent organic light-emitting diodes (PHOLED).[4] Among the great variety of ligands, the most common chelators are 2,2′-bipyridines (bpy), 1.10-phenanthrolines (phen), 2,2′,6′,2″-terpyridines (tpy), and their derivatives. Besides these systems bearing two or more N-heteroatom rings, bisdiazine ligands are of special interest because they represent chelating ligands leading to complexes (Ru(II) complexes particularly) with higher photostabilities toward metal-ligand photodissociation, compared to bipyridine analogues.[5] This is due to the strong "back-bonding" (good π- acceptor and σ-donor ability) toward π-electron rich metal fragments, and to a substantially lower lowest unoccupied molecular orbital (LUMO) energy level by comparison with that of many of the previous bipyridine derivatives.[5a,6] Despite these interesting features, until now, little attention has

*To whom correspondence should be addressed. Phone: +33(0)1 44 27 53 02. Fax: +33 (0)1 44 27 70 89. E-mail: andre-jean.attias@upmc.fr.

(1) (a) Lehn, J.-M. In *Supramolecular Chemistry: Concepts and Perspectives*; VCH: Weinheim, Germany, 1995. (b) Lehn, J.-M. *Chem. Soc. Rev.* **2007**, *36*, 151–160.

(2) (a) Deisenhofer, J.; Epp, O.; Miki, K.; Huber, R.; Michel, H. *Nature* **1986**, *318*, 618–624. (b) Hoertz, P. G.; Staniszewski, A.; Marton, A.; Higgins, G. T.; Incarvito, C. D.; Rheingold, A. L.; Meyer, G. J. *J. Am. Chem. Soc.* **2006**, *128*(25), 8234–8245. (c) Meylemans, H. A.; Lei, C.-F.; Damrauer, N. H. *Inorg. Chem.* **2008**, *47*, 4060–4076. (d) Fukuzumi, S. *Eur. J. Inorg. Chem.* **2008**, 1351–1362.

(3) (a) O'Reagan, B.; Grätzel, M. *Nature* **1991**, *353*, 737–740. (b) Jang, S.-R.; Yum, S.-R.; Klein, C.; Kim, K.-J.; Wagner, P.; Officer, D.; Grätzel, M.; Nazeeruddin, M. K. *J. Phys. Chem. C* **2009**, *113*, 1998–2003. (c) Grabulosa, A.; Beley, M.; Gros, P. C.; Cazzanti, S.; Caramori, S.; Bignozzi, C. A. *Inorg. Chem.* **2009**, *48*, 8030–8036. (d) Subbaiyan, N. K.; Wijesinghe, C. A.; D'Souza, F. *J. Am. Chem. Soc.* **2009**, *131*, 14646–14647. (e) Grätzel, M.; Durrant, J. R. In *Series on Photoconversion of Solar Energy*; Archer, M. D., Nozik, A. J., Eds.; World Scientific: Singapore, 2009; Vol. *3*, pp 503−538.

(4) (a) Baldo, M. A.; You, Y.; Shoustikov, A.; Sibley, S.; Thompson, M. E.; Forrest, S. R. *Nature* **1998**, *395*, 151–154. (b) O'Brien, D. F.; Baldo, M. A.; Thompson, M. E.; Forrest, S. R. *Appl. Phys. Lett.* **1999**, *74*, 442–444. (c) Baldo, M. A.; Lamansky, S.; Burrows, P. E.; Thompson, M. E.; Forrest, S. R. *Appl. Phys. Lett.* **1999**, *75*, 4–6. (d) Tung, Y.-L.; Wu, P.-C.; Liu, C.-S.; Chi, Y.; Yu, J.-K.; Hu, Y.-H.; Chou, P.-T.; Peng, S.-M.; Lee, G.-H.; Tao, Y.; Carty, A. J.; Shu, C.-F.; Wu, F.-I. *Organometallics* **2004**, *23*, 3745–3748. (e) Lee, S.-J.; Park, J.-S.; Song, M.; Shin, I. A.; Kim, Y.-I.; Lee, J. W.; Kang, J.-W.; Gal, Y.-S.; Kang, S.; Lee, J. Y.; Jung, S.-Y.; Kim, H.-S.; Chae, M.-Y.; Jin, S.-H. *Adv. Funct. Mater.* **2009**, *19*, 2205–2212.

(5) (a) Ernst, S.; Kaim, W. *Inorg. Chim. Acta* **1986**, *114*, 123–125. (b) Dürr, H.; Schwarz, R.; Andreis, C.; Willner, I. *J. Am. Chem. Soc.* **1993**, *115*, 12362–12365. (c) Berger, S.; Klein, A.; Kaim, W.; Fiedler *J. Organomet. Chem.* **1986**, *302*, 211–215.

(6) Ernst, S.; Kaim, W. *Angew. Chem.* **1985**, *97*, 431–433.

Published on Web 04/02/2010

Chart 1. Structures of (a) Previous 6,6′-(Disubstituted)-3,3′-bipyridine, and (b) Novel 3,3′-Bipyridazine Ligand **L**

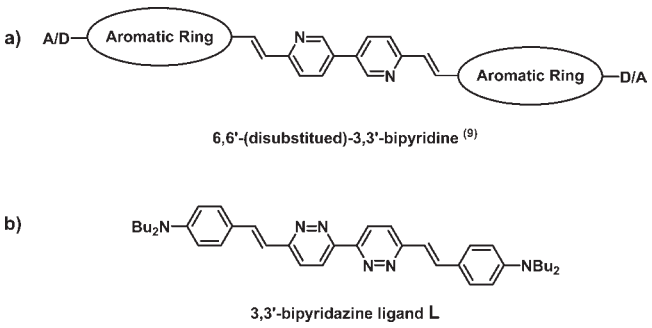

been given to complexes bearing bisdiazine ligands, more particularly 3,3′-bipyridazine.[7] Besides oligo(pyridazine) structures,[8] more surprisingly, to our knowledge, there is no work related to extended π-conjugated 3,3′-bipyridazine ligand. The potential interest of this design is the expected tuning of the photophysical and electronic properties by modulating the conjugation length and the nature of end-capping groups.

Previously, we developed a new class of multifunctional extended π-conjugated symmetric and unsymmetric 6,6′-(disubstituted)-3,3′-bipyridine based chromophores (Chart 1a).[9] Depending on the π-conjugated bridge and by varying the nature of the acceptor(A)/donor(D) end-capping groups, we were then able to tune the polymorphism,[9a,b] electrochemical and photoluminescent characteristics, and second- as well as third order non linear optical (NLO) properties of this class of chromophores.[9c−f] As an application, lasing properties were demonstrated, and a blue-OLED was fabricated.[9i] Unfortunately, these materials are not suitable for metal-ion binding, preventing their use as metal-ion sensing fluorophores or as ligand for the formation of coordination complexes.

In this context, here we pursued a new design strategy for fluorescent ion responsive molecules capable of metal-ion binding. More specifically, we defined a new class of π-conjugated ligands by replacing the 3,3′-bipyridine acceptor core with the more electron withdrawing 3,3′-bipyridazine core (Chart 1b), expecting that the two added nitrogen atoms should take part in metal binding.

More precisely, we report on the design and synthesis of a new centrosymmetric π-conjugated 6,6′-distyryl-3,3′-bipyridazine based ligand **L** (Chart 1b) with extended conjugation length, end-capped with terminal dibutylamino groups on both ends. Thus we created a quadrupolar donor−acceptor−donor (D-A-D) motif with an expected symmetrical charge-transfer from the external electron-donor amino groups of the molecule to the central 3,3′-bipyridazine core acting as an electron-acceptor moiety. We present the electrochemical and photophysical (absorption and emission) properties of **L**, as well as the use of this new compound in a green OLED. Moreover, the ability of this ligand to complex metallic centers (Cu^{I}, Ni^{II}, Pt^{II}, and Ir^{III}) was also investigated (Chart 2) to access different geometries and to tune their electronic and optical properties.

Experimental Section

General Considerations. ^{1}H NMR and ^{13}C NMR spectra were recorded at 250 and 63 MHz respectively. Proton chemical shifts (δ) are reported in parts per million (ppm) downfield from tetramethylsilane ($SiMe_4$). Quantum Chemistry Calculations were performed using the Gaussian 03W package.[10] Gas phase geometries and electronic energies were calculated by full optimization without imposed symmetry of the conformations using the B3LYP density functional,[11] with the 6-31G* basis set,[12] starting from preliminary optimizations performed with semi-empirical AM1 methods. The Onsager radius[10b] a was then estimated from the radius of the equivalent sphere with a molecular volume defined as the volume inside a contour of 0.001 electrons/bohr^3 density + 0.5 Å as recommended for the Onsager solvent reaction field model.[10c] Cyclic Voltammetry experiments were performed with a three-electrode setup using a platinum counter-electrode and a reference electrode. The reference electrode was an aqueous saturated calomel electrode with a salt bridge containing the supporting electrolyte. The working electrode was either disks of glassy carbon (∅ 0.8 mm, Tokai Corp.), gold (∅ 1 mm), or platinum (∅ 1 mm). The working electrodes were carefully polished before each set of voltammograms with 1 μm diamond paste and cleansed in an ultrasonic bath with dichloromethane. The electrochemical instrumentation consisted of a PAR Model 175 Universal programmer and of a home-built potentiostat equipped with a positive feedback compensation device. The data were acquired with a 310 Nicolet oscilloscope. The potential values were

(7) (a) Kropf, M.; Dürr, H.; Collet, C. *Synthesis* **1996**, *5*, 609–613. (b) Kropf, M.; Joselevich, E.; Dürr, H.; Willner, I. *J. Am. Chem. Soc.* **1996**, *118*, 655–665. (c) Kropf, M.; Van Loyen, D.; Schwarz, O.; Dürr, H. *J. Phys. Chem. A* **1998**, *102*, 5499–5505. (d) Schwarz, O.; Van Loyen, D.; Jockush, S.; Turro, N. J.; Dürr, H. *J. Photochem. Photobiol. A: Chem.* **2000**, *132*, 91–98. (e) Gardner, J. S.; Strommen, D. P.; Szulbinski, W. S.; Su, H.; Kincaid, J. R. *J. Phys. Chem. A* **2003**, *107*, 351–357.

(8) (a) Baxter, P. N. W.; Lehn, J.-M.; Fisher, J.; Youinou, M.-T. *Angew. Chem., Int. Ed.* **1994**, *33*, 2284–2287. (b) Baxter, P. N. W.; Lehn, J.-M.; Baum, G.; Fenske, D. *Chem.—Eur. J.* **2000**, *6*, 4510–4517. (c) Marquis, A.; Kintzinger, J.-P.; Graff, R.; Baxter, P. N. W.; Lehn, J.-M. *Angew. Chem., Int. Ed.* **2002**, *41*, 2760–2764. (d) Bouffard, J.; Eaton, R. F.; Müller, P.; Swager, T. M. *J. Org. Chem.* **2007**, *72*, 10166–10169.

(9) (a) Attias, A.-J.; Cavalli, C.; Bloch, B.; Guillou, N.; Noel, C. *Chem. Mater.* **1999**, *11*, 2057–2068. (b) Attias, A.-J.; Hapiot, P.; Wintgens, V.; Valat, P. *Chem. Mater.* **2000**, *12*, 461–471. (c) Lemaitre, N.; Attias, A.-J.; Ledoux, I.; Zyss, J. *Chem. Mater.* **2001**, *13*, 1420–1427. (d) Chérioux, F.; Attias, A.-J.; Maillotte, H. *Adv. Funct. Mater.* **2002**, *12*, 203–208. (e) Chen, Q.; Sargent, E. H.; Leclerc, N.; Attias, A.-J. *Appl. Phys. Lett.* **2003**, *82*, 4420–4422. (f) Chen, Q.; Sargent, E. H.; Leclerc, N.; Attias, A.-J. *Appl. Opt.* **2003**, *42*, 7235–7241. (g) Leclerc, N.; Serieys, I.; Attias, A.-J. *Tetrahedron Lett.* **2003**, *44*, 5879–5882. (h) Leclerc, N.; Galmiche, L.; Attias, A.-J. *Tetrahedron. Lett.* **2003**, *44*, 5883–5887. (i) Leclerc, N.; Sanaur, S.; Galmiche, L.; Mathevet, F.; Attias, A.-J.; Fave, J.-L.; Roussel, J.; Hapiot, P.; Lemaitre, N.; Geffroy, B. *Chem. Mater.* **2005**, *17*, 502–513.

(10) (a) Frisch, M. J.; Trucks, G. W.; Schlegel, H. B.; Scuseria, G. E.; Robb, M. A.; Cheeseman, J. R.; Montgomery Jr., J. A.; Vreven, T.; Kudin, K. N.; Burant, J. C.; Millam, J. M.; Iyengar, S. S.; Tomasi, J.; Barone, V.; Mennucci, B.; Cossi, M.; Scalmani, G.; Rega, N.; Petersson, G. A.; Nakatsuji, H.; Hada, M.; Ehara, M.; Toyota, K.; Fukuda, R.; Hasegawa, J.; Ishida, M.; Nakajima, T.; Honda, Y.; Kitao, O.; Nakai, H.; Klene, M.; Li, X.; Knox, J. E.; Hratchian, H. P.; Cross, J. B.; Adamo, C.; Jaramillo, J.; Gomperts, R.; Stratmann, R. E.; Yazyev, O.; Austin, A. J.; Cammi, R.; Pomelli, C.; Ochterski, J. W.; Ayala, P. Y.; Morokuma, K.; Voth, G. A.; Salvador, P.; Dannenberg, J. J.; Zakrzewski, V. G.; Dapprich, S.; Daniels, A. D.; Strain, M. C.; Farkas, O.; Malick, D. K.; Rabuck, A. D.; Raghavachari, K.; Foresman, J. B.; Ortiz, J. V.; Cui, Q.; Baboul, A. G.; Clifford, S.; Cioslowski, J.; Stefanov, B. B.; Liu, G.; Liashenko, A.; Piskorz, P.; Komaromi, I.; Martin, R. L.; Fox, D. J.; Keith, T.; Al-Laham, M. A.; Peng, C. Y.; Nanayakkara, A.; Challacombe, M. Gill, P. M. W.; Johnson, B.; Chen, W.; Wong, M. W.; Gonzalez, C. Pople, J. A. *Gaussian 03*, Revision B.04; Gaussian, Inc.: Pittsburgh, PA, 2003. (b) Onsager, L. *J. Am. Chem. Soc.* **1936**, *58*, 1486–1493. (c) Wong, M. W.; Wiberg, K. B.; Frisch., M. J. *J. Am. Chem. Soc.* **1992**, *114*, 1645–1652.

(11) Becke, A. D. *J. Chem. Phys.* **1993**, *98*, 5648–5652.

(12) Hariharan, P. C.; Pople, J. A. *Chem. Phys. Lett.* **1972**, *16*, 217–219.

Chart 2. Complexes Structures

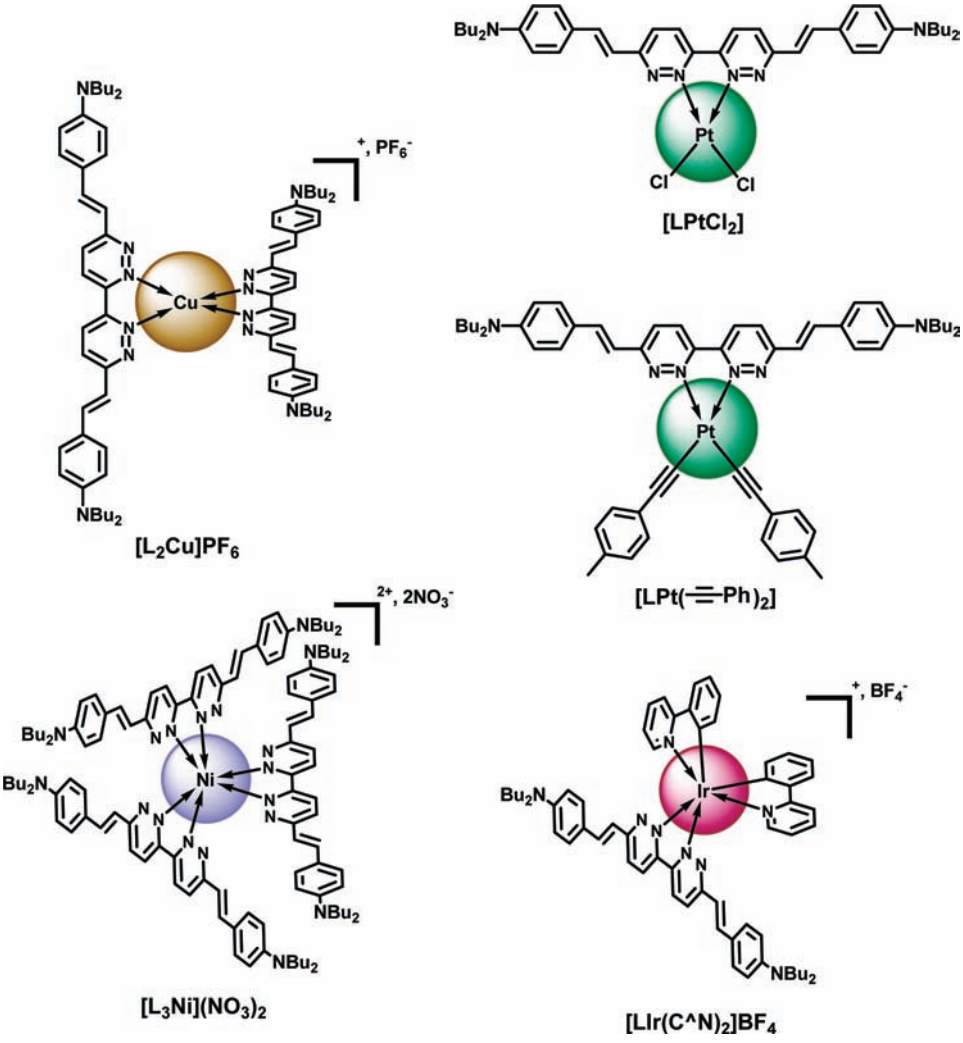

internally calibrated against the ferrocene/ferricinium couple (E° = 0.405 V vs SCE) for each experiment. All the cyclic voltammetry experiments were carried out at 20 °C using a cell equipped with a jacket allowing circulation of water from the thermostat. Oxygen was removed from all solutions by bubbling argon. The solvent was a toluene/acetonitrile mixture (50/50 v/v), and the supporting electrolyte was tetrabutylammonium tetrafluoroborate (Fluka, Puriss) at a concentration of 0.1 mol·L^{-1}. Acetonitrile was from Merck, (Uvasol quality less than 0.01% of water) and toluene from Prolabo (R.P. Normapur). The UV−visible absorption spectra were obtained in different solvents and solvent mixtures with Avaspec spectroscopy (S:Avaspec-2048, D:Avalight-DHS). Appropriate concentrations (absorbance below 0.2 au) were chosen to avoid inner filter effects. The fluorescence emission spectra in the 450−800 nm region were obtained from the same sample used for absorption measurements, using a Luminescence spectrometer 'LS55' (PerkinElmer). To minimize the atmospheric H_2O and O_2 contamination in the sample, argon gas was purged through the solution before measurements. The scan speed was fixed at 500 nm min^{-1}. Molar absorption coefficients (ε_{max}) were determined using the Beer−Lambert law. Fluorescence quantum yields were determined in different solvents by using 2,4,6-triphenylpyrylium tetrafluoroborate (in dichloromethane under argon, ϕ_{ref} = 0.58) as a reference.[13] The quantum yield of the sample was determined using the equation

$$\phi = \phi_{ref}\left(\frac{I_{ref}}{I}\right)\left(\frac{n}{n_{ref}}\right)^2\left(\frac{A_{ref}}{A}\right)$$

where ϕ is the relative quantum yield of sample, I is the integrated intensity of fluorescence spectrum of sample, A is the intensity of absorbance spectrum of sample, and n is the refractive index. The subscript *ref* refers to the value of the reference fluorescence material of known quantum yield. Luminescence quantum yields in the 650−800 nm region were measured at room temperature in Argon deaerated solution relative to Cresyl violet in ethanol (ϕ_F = 0.51; λ_{EX} = 578 nm),[14] and tetramethoxy-bis-isoindolodipyrromethene-difluoroborate in dichloromethane (ϕ_F = 0.41; λ_{Ex} = 660 nm).[15] Quantum yields were corrected for the change in refractive index between the chosen solvent and dichloromethane solution. Luminescence studies for the platinum and iridium complexes were made with a Jobin-Yvon Fluoromax 4 spectrometer and the emission spectra were automatically corrected from the detector response. As given by the constructor the correction is less accurate above 850 nm. The configuration of the OLED

(13) Melhuish, W. H. *J. Phys. Chem.* **1961**, *65*, 229–235.

(14) Olmsted, J., III *J. Phys. Chem.* **1979**, *83*, 2581–2584.

(15) Ulrich, G.; Goeb, S.; De Nicola, A.; Retailleau, P.; Ziessel, R. *Synlett.* **2007**, *10*, 1517–1520.

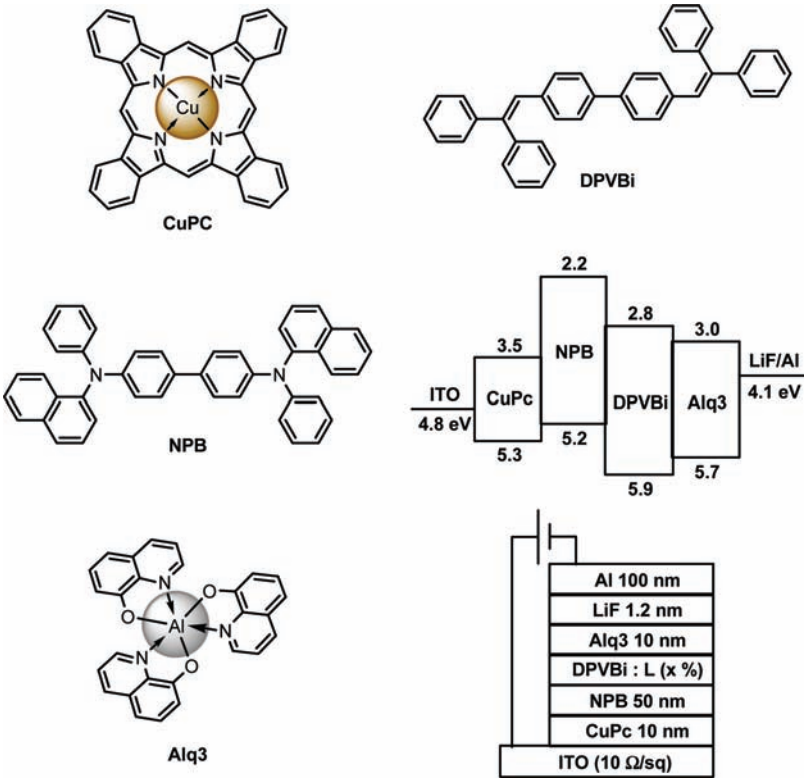

Figure 1. Device structure, energy level diagram of the OLED, and chemical structure of its components.

device, depicted in Figure 1 was ITO/CuPc/NPB/(DPVBi:L (× wt %))/Alq3/LiF/Al. The chemical structure and the highest occupied molecular orbital (HOMO) and the LUMO energy levels of the diode components are also presented in Figure 1.[16] CuPc is copper phthalocyanine as a buffer layer, α-NPB is *N*,*N*′-bis(naphthalen-1-yl)-*N*,*N*′-bis(phenyl)benzidine as a hole transporting layer, DPVBi is 4,4′-bis(2,2-diphenyl-vinyl)-1,1′-biphenyl as a host, Alq3 is tris(8-hydroxyquinolato) aluminum as an electron transporting layer. The EL device was fabricated as follow. ITO-coated glass substrates (with a sheet resistance of 10 Ω/sq) were first cleaned by successive ultrasonic treatments in detergent, deionized water, and ethanol. After that chemical cleaning, the substrates were treated by irradiation in a UV/Ozone chamber for 30 mn. The organic materials (from Aldrich and Syntec) and the cathode LiF/Al were sequentially deposited by sublimation under high vacuum ($< 10^{-6}$ Torr) at a rate of 0.2−0.3 nm s^{-1}. The entire device is fabricated in the same run without breaking the vacuum. The active area of the devices defined by the overlap of the ITO anode and the metallic cathode was 0.3 cm^2. The emissive layer of (DPVBi:**L**) was made by co-evaporation of the two products from different sources. The I-V-L characteristics of the diodes were measured with a regulated power supply (ACT 100 Fontaine) combined with a multimeter (I-V) and a 1 cm^2 area silicon calibrated photodiode (Hamamatsu). The spectral emissions (Commission Internationale de l'Eclairage (CIE) coordinates) were recorded with a spectrophotometer (SpectraScan PR650). All the measurements were performed under ambient conditions. All reagents were purchased from commercial suppliers and used without further purification. Flash chromatography was carried out with silica gel (Merck, Si 60, 40−63 μm). Thin layer chromatography (TLC) was performed with use of aluminum silica gel sheets (60 F254, Merck). $[Pt(DMSO)_2Cl_2]$,[17] $[Ir(C^N)_2Cl]_2$[18] were synthesized according to the literature procedures and yielded satisfactory mass and ^1H NMR spectra.

Ligand Synthesis. 4,4′-(1*E*,1′*E*)-2,2′-(3,3′-bipyridazine-6,6′-diyl)bis(ethene-2,1-diyl)bis(*N*,*N*-dibutylaniline) (L). A solution of 6,6′-dimethyl-3,3′-bipyridazine (4 g, 21.48 mmol), 4-(dibutylamino)-benzaldehyde (10.5 g, 45.00 mmol), and catalytic amount of 4-methylbenzenesulfonic acid (20 mg, 0.12 mmol) was stirred under N_2 at reflux. After 12 h, another portion of 4-methylbenzenesulfonic acid (20 mg, 0.12 mmol) was then added, and the mixture was stirred at reflux for an additional 12 h. The reaction mixture was then cooled to room temperature, and solvent was removed under vacuum. The organic layer was washed with water, dried over $MgSO_4$, and evaporated to dryness. Column chromatography (SiO_2, Et_2O/Hexane = 3/97) and recrystallization in EtOH gave **L** as an orange solid with 25% yield. ^1H NMR (250 MHz, $CDCl_3$): δ 0.99 (t, 12H, $^3J(H,H) = 6.9$ Hz), 1.44 (qt, 8H, $^3J(H,H) = 6.9$ Hz, $^3J(H,H) = 6.9$ Hz), 1.61 (tt, 8H, $^3J(H,H) = 6.9$ Hz), 3.32 (t, 8H, $^3J(H,H) = 6.9$ Hz), 6.66 (d, 4H, $^3J(H,H) = 9.3$ Hz), 7.17 (d, 2H, $^3J(H,H) = 16.1$ Hz), 7.50 (d, 4H, $^3J(H,H) = 9.3$ Hz), 7.68 (dd, 2H, $^3J(H,H) = 9.3$ Hz), 7.71 (d, 2H, $^3J(H,H) = 16.1$ Hz), 8.70 (d, 2H, $^3J(H,H) = 9.3$ Hz); $^{13}C\{^1H\}$ NMR (100.6 MHz, $CDCl_3$): δ: 14.0, 20.4, 26.0, 50.7, 110.7, 118.7, 123.3, 13.9, 124.0, 129.3, 136.3, 148.7, 154.0, 158.3; Elem anal. Found (%): C, 77,94; H, 8.61; N, 13.45. calcd for $C_{40}H_{52}N_6$: C, 77.88; H, 8.50; N, 13.52. mp = 214.5 °C.

Complexes Synthesis. Complex $[L_2Cu]PF_6$. A suspension of the free bipyridazine based ligand L (171 mg, 0.277 mmol) in anhydrous DMF (10 mL) was stirred under N_2 at 60 °C. After 30 min, a solution of $Cu(MeCN)_4PF_6$ (52 mg, 0.139 mmol) in anhydrous DMF (2 mL) was then added, and the mixture was stirred at reflux for 12 h. The reaction mixture was then cooled to room temperature, and solvent was removed under vacuum. The crude product was taken up in acetone (5 mL) and was

(16) Hosokawa, C.; Higashi, H.; Nakamura, H.; Kusumoto, T. *Appl. Phys. Lett.* **1995**, *67*, 3853–3855.
(17) Price, J. H.; Birk, J. P.; Wayland, B. B. *Inorg. Chem.* **1978**, *17*, 2245–2250.
(18) Sprouse, S.; King, K. A.; Spellane, P. J.; Watts, R. J. *J. Am. Chem. Soc.* **1984**, *106*, 6647–6653.

Scheme 1. Synthetic Route of **L**

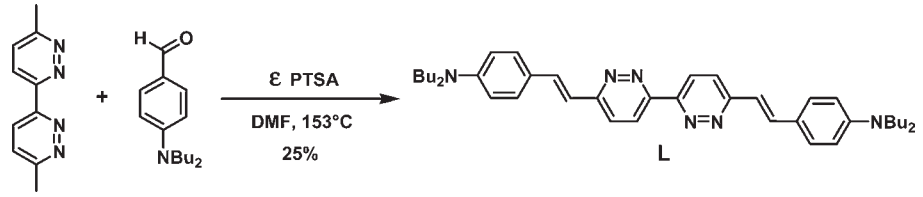

precipitate in hexane (100 mL). Several precipitations with acetone/hexane (v/v = 1/20) gave **[L_2Cu]PF_6** as a dark purple solid in 95% yield. Elem anal. found (%): C, 66.41; H, 7.00; N, 11.32. calcd. for $C_{80}H_{104}N_{12}PF_6Cu$: C, 66.62; H, 7.27; N, 11.65; P, 2.15; F, 7.90; Cu, 4.41. MS ESI+ *m*/*z*: calcd for $C_{80}H_{104}N_{12}Cu^+$ 1295.78 Da found 1295.9 Da.

Complex [L_3Ni]$(NO_3)_2$. A suspension of the free bipyridazine based ligand **L** (110 mg, 0.178 mmol) in anhydrous DMF (8 mL) was stirred under N_2 at 60 °C. After 30 min, a solution of Ni$(NO_3)_2 \cdot 6H_2O$ (17.3 mg, 0.059 mmol) in anhydrous DMF (3 mL) was then added, and the mixture was stirred at reflux for 12 h. The reaction mixture was then cooled to room temperature, and solvent was removed under vacuum. The crude product was taken up in acetone (5 mL) and was precipitated in diethylether (100 mL). Several precipitations with acetone/diethylether (v/v = 1/20) gave **[L_3Ni]$(NO_3)_2$** as a dark purple solid in 90% yield. Elem anal. found (%): C, 69.39; H, 7.52; N, 13.27. calcd. for $C_{120}H_{156}N_{20}O_6Ni \cdot 2H_2O$: C, 69.65; H, 7.79; N, 13.54. MS ESI+ *m*/*z*: calcd for $C_{120}H_{156}N_{18}Ni^{2+}$ 954.11 Da found 954.3 Da.

Complex [LPtCl_2]. A Schlenk flask was charged with the appropriate [Pt$(DMSO)_2Cl_2$] precursor (94 mg, 0.223 mmol), ligand **L** (110 mg, 0.178 mmol), and tetrahydrofuran (THF, 15 mL). The solution was degassed for 15 min with argon and heated at 60 °C during 2 h. During the course of the reaction the color of the solution progressively turned dark purple and after a short time thin layer chromatography revealed the absence of free ligand. After cooling the solution the solvent was rotary evaporated, and the residue was purified by column chromatography, on flash silica using a mixture of CH_2Cl_2/methanol as mobile phase (gradient from 0.2 to 1.0% methanol). Recrystallization was ensured by slow diffusion of diethylether in a dichloromethane solution. Complex **[LPtCl_2]** was obtained as a dark blue solid (145 mg, 92%). ^{1}H NMR (400.1 MHz, d_2-dichloromethane): δ 7.97 (d, ^3J = 8 Hz, 2H), 7.89 (d, ^3J = 8 Hz, 2H), 7.59 (d, ^3J = 16 Hz, 2H), 7.38 (d, ^3J = 8 Hz, 4H), 6.81 (d, ^3J = 16 Hz, 2H), 6.56 (d, ^3J = 8 Hz, 4H), 3.26 (d, ^3J = 7.5 Hz, 8H), 1.57 (m, 8H), 1.37 (m, 8H), 0.97 (t, ^3J = 7.5 Hz, 12H) ; ^{13}C{^{1}H} NMR (100.6 MHz, d_2-dichloromethane): δ 160.1, 153.8, 149.3, 135.2, 130.5, 128.8, 125.7, 122.5, 116.4, 111.4, 52.6, 29.4, 20.3, 13.7 ; ES-MS *m*/*z* (nature of the peak, relative intensity): 884.3 ([M+H]$^+$, 100), 883.3 ([M+H]$^+$, 90), 881.2 ([M+H]$^+$, 70); Anal. Calcd for $C_{40}H_{52}N_6PtCl_2$: C, 54.42; H, 5.94; N, 9.52. Found: C, 54.19; H, 5.67; N, 9.32; UV−vis (CH_2Cl_2) λ (nm), ε (M^{-1} cm^{-1}): 255 (12500), 330 (20200), 488 (32300), 608 (48000).

Complex [LPt(-≡-Ph)$_2$]. A Schlenk flask was charged with **[LPtCl_2]** (65 mg, 0.074 mmol), and tolylacetylene (36 mg, 0.309 mmol), and a mixture of dichloromethane/triethylamine (10/3 mL). The solution was vigorously degassed for 30 min with argon. Then CuI (1.4 mg, 0.0074 mmol) was added under argon as a solid. During the course of the reaction the color of the solution progressively turned violet. After 24 h the reaction was quenched with water, and the solution evaporated to dryness. Purification was ensured by column chromatography on flash silica using a mixture of CH_2Cl_2/methanol as mobile phase (gradient from 0.2 to 0.5% methanol). Recrystallization was ensured by slow evaporation of dichloromethane from a dichloromethane/cyclohexane solution. Complex **[LPt(-≡-Ph)$_2$]** was obtained as a dark violet solid (60 mg, 77%). ^{1}H NMR (400.1 MHz, d_2-dichloromethane): δ 7.82 (d, ^3J = 8.8 Hz, 2H),

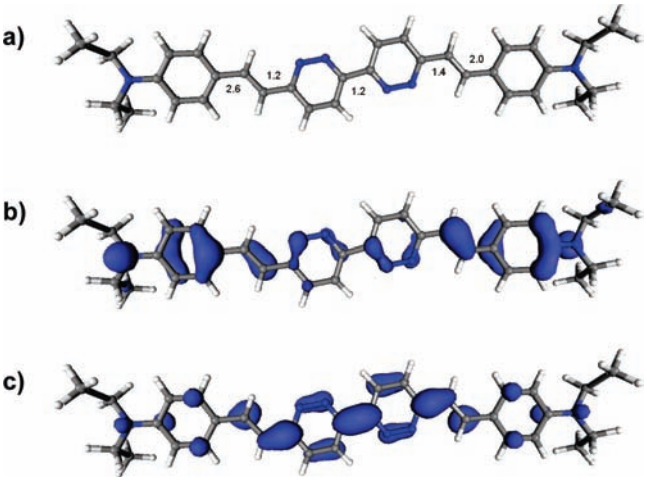

Figure 2. Optimized B3LYP/6-31G* geometry for **L** analogue (N(Ethyl)$_2$ terminal groups). (a) Numbers are the adjacent dihedral angles; (b) HOMO and (c) LUMO molecular orbitals.

7.64 (d, ^3J = 8.8 Hz, 2H), 7.22 (d, ^3J = 15.8 Hz, 2H), 7.49 (d, ^3J = 8.0 Hz, 4H), 7.18 (d, ^3J = 8 Hz, 4H), 7.03 (d, ^3J = 8.8 Hz, 4H), 6.63 (d, ^3J = 15.8 Hz, 2H), 6.42 (d, ^3J = 8.8 Hz, 4H), 3.21 (t, ^3J = 7.5 Hz, 8H), 2.44 (s, 6H), 1.55 (m, 8H), 1.34 (m, 8H), 0.97 (t, ^3J = 7.5 Hz, 12H); ^{13}C{^{1}H} NMR (100.6 MHz, d_2-dichloromethane): δ 159.9, 153.6, 149.5, 139.0, 135.0, 131.8, 130.1, 128.8, 127.1, 125.9, 125.7, 122.2, 116.4, 111.1, 102.8, 86.9, 50.6, 29.4, 21.1, 20.2, 13.7 ; ES-MS *m*/*z* (nature of the peak, relative intensity): 1043.3 ([M+H]$^+$, 100), 1042.3 ([M+H]$^+$, 100), 1041.3 ([M+H]$^+$, 60) ; Anal. Calcd for $C_{58}H_{66}N_6Pt$: C, 66.84; H, 6.38; N, 8.06. Found: C, 66.52; H, 6.21; N, 7.84 ; UV−vis (CH_2Cl_2) λ (nm), ε (M^{-1} cm^{-1}): 267 (31200), 330 (18100), 498 (sh, 34700), 556 (38800).

Complex [Ir(C^N)$_2$]BF_4. A Schlenk flask was charged with L (66 mg, 0.107 mmol), and the μ-chloro-Ir-dimer [Ir(C^N)$_2$Cl]$_2$ (57 mg, 0.053 mmol), and dichloromethane (10 mL). The solution was degassed for 10 min with argon and heated at 50 °C. TLC was used to follow the progress of the reaction. During the course of the reaction the color of the solution progressively turned deep-red. After one night the reaction was quenched with water and the solution evaporated to dryness. The residue was dissolved in the minimum *N*,*N*-dimethylformamide (DMF, 5 mL) and dropwise added via a pipette filled with Celite to an aqueous solution (10 mL) containing $NaBF_4$ (500 mg). During the addition a voluminous precipitate formed. After 1 h stirring at room tempertaure (rt), the suspension was filtered over paper and washed with water (3×100 mL). Natural drying was ensured under the fumehood. Purification was performed by column chromatography, on alumina deactivated with 6% water using a mixture of CH_2Cl_2/methanol as mobile phase (gradient from 1 to 1.5% methanol). Recrystallization was ensured by slow diffusion of diethylether in a dichloromethane solution. The **[Ir(C^N)$_2$]BF_4** complex was obtained as a dark violet solid (89 mg, 69%). ^{1}H NMR (400.1 MHz, d_2-dichloromethane): δ 8.61 (d, ^3J = 9.0 Hz, 2H), 7.93 (d, ^3J = 8.2 Hz, 2H), 7.76 (m, 4H), 7.71 (d, ^3J = 9.2 Hz, 2H), 7.65 (d, ^3J = 5.6 Hz, 2H), 7.30 (d, ^3J = 9.2 Hz, 4H), 7.27 (d, ^3J = 16 Hz, 2H),), 7.14 (t, ^3J = 7.2 Hz, 2H),

Table 1. Maximum Absorption and Emission Energies, Quantum Yield of Ligand **L** in Solution in Several Solvent and Solvent Parameter Values

	absorption			emission						
	λ_{abs}		ε_{max}	λ_{em}		Stokes shift	polarity		refraction index	quantum yield
solvent	(nm)	(eV)	(L mol^{-1} cm^{-1})	(nm)	(eV)	(eV)	$\varepsilon^{22,23}$	$\Delta f^{22,23}$	$n^{22,23}$	Φ (%)
n-hexane	422	2.935	64700	461	2.689	0.246	1.88	0.000411	1.37	
toluene	436	2.844	64700	495	2.505	0.339	2.38	0.012311	1.50	73
diethyl ether	430	2.880	70200	504	2.455	0.425	4.20	0.163353	1.35	43
chloroform	454	2.731	72150	533	2.324	0.407	4.80	0.149038	1.45	97
ethyl acetate	436	2.844	67850	539	2.300	0.544	6.02	0.200506	1.37	80
dichloromethane	453	2.737	71250	557	2.226	0.511	8.93	0.218511	1.42	85
2-butanone	443	2.799	71200	579	2.139	0.659	18.11	0.271627	1.38	18
ethanol	456	2.719	72600	602	2.059	0.659	24.55	0.289263	1.36	13
acetonitrile	443	2.799	73650	605	2.049	0.750	35.94	0.30613	1.34	32

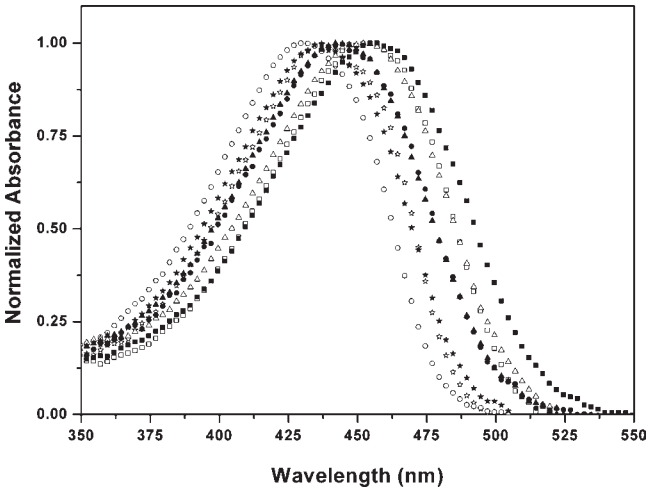

Figure 3. Normalized absorption spectra of **L** (0.6×10^{-5} M) in several solvents at 25 °C. Toluene (☆), diethylether (○), dichloromethane (△), chloroform (□), ethylacetate (★), 2-butanone (●), acetonitrile (▲), and ethanol (■).

6.98 (m, 4H), 6.68 (d, $^3J = 16$ Hz, 2H), 6.61 (d, $^3J = 9.0$ Hz, 4H), 6.39 (d, $^3J = 7.2$ Hz, 2H), 3.32 (t, $^3J = 7.6$ Hz, 8H), 1.60 (m, 8H), 1.38 (m, 8H), 0.97 (t, $^3J = 7.5$ Hz, 12H); $^{13}C\{^1H\}$ NMR (100.6 MHz, d_2-Dichloromethane): δ 168.2, 161.3, 154.2, 149.9, 149.2, 143.7, 139.8, 137.9, 131.7, 129.9, 129.7, 128.0, 125.9, 125.5.3, 124.1, 123.0, 122.0, 121.9, 119.6, 115.7, 111.4, 50.7, 29.4, 20.3, 13;72 ; ES-MS *m*/*z* (nature of the peak, relative intensity): 1117.3 ($[M]^+$, 100); Anal. Calcd for $C_{62}H_{68}N_8IrBF_4$: C, 61.83; H, 5.69; N, 9.30. Found: C, 61.47; H, 5.34; N, 9.13 ; UV−vis (CH_2Cl_2) λ (nm), ε (M^{-1} cm^{-1}): 253 (41800), 314 (28900), 575 (60800).

Results and Discussion

Ligand Synthesis. The symmetrical quadrupolar molecule **L** was conveniently prepared via a Knoevenagel condensation, under acidic conditions, as outlined in Scheme 1. 6,6′-Dimethyl-3,3′-bipyridazine (**1**) was synthesized by adapting the homocoupling of halopyridines mediated by nickel-phosphine complexes,[9a,19] with 3-chloro-6-methylpyridazine as starting material. Thus **L** was obtained in a one-pot reaction by reacting one mole of (**1**) with two moles of the 4-(dibutylamino)benzaldehyde, and isolated in 25% yield as a bright-orange powder. The structures and purity of all the compounds were confirmed by using ^1H and ^{13}C NMR spectroscopy. The *trans* stereochemistry of **L** was clearly established, based on the coupling constants (15.6 Hz) in the ^1H NMR spectra of the protons on the olefinic carbons.

Quantum Chemical Calculations. To gain better insight into the geometry and electronic properties of the molecule **L**, quantum-chemical calculations were performed at the B3LYP/6-31G* level in the density functional theory (DFT) formalism. The optimized ground-state geometry of the analogue of **L** (terminal butyl chains have been replaced by ethyl groups) is reported in Figure 2a. First of all, this molecule adopts an almost rigid planar structure, the dihedral angle between the two pyridazine rings being smaller than 1.2°, while the pyridazine and phenyl rings are in the same plane (pyridazine-vinyl and phenyl-vinyl twist angles between 1.2 and 1.4° and 2.0−2.6°, respectively). Consequently, this elongated planar molecule (22.84 Å between the two final $N(Et)_2$ groups) is centrosymmetric and has no dipolar moment. It should be noted that this molecule is more planar than its 3,3′-bipyridine based analogue, for which the dihedral angle between the pyridine rings is 34.6° corresponding to a twisted conformation in the ground state. Second, the bond-length alternation (BLA) parameter,[20] defined as the difference between single and double bonds on the vinyl bridge, is 0.106 Å. Since this value is close to the polyene limit, this high degree of bond length alternation is indicative of a low contribution of the charge-separation resonance form to the ground-state configuration of **L**.[20] Third, the HOMOs and LUMOs exhibit a specific pattern (Figure 2b,c). The HOMO orbital is mainly localized at the terminal rings, whereas a reversed pattern is observed for the LUMO which is mostly located at the central pyridazine rings. According to the electron localization in HOMO and LUMO, the one-photon transition from the ground state (S_0) to the lowest excited state (S_1) should contribute to a polar property of (S_1), explaining the observed solvatochromism in one-photon excitation experiments, despite the centrosymmetric geometry in the ground state S_0, as reported with other D-A-D systems.[21]

(19) Tiecco, M.; Testaferri, L.; Tingoli, M.; Chianelli, D.; Montanucci, M. *Synthesis* **1984**, *9*, 736–737.

(20) Marder, S. R.; Perry, J. W.; Bourhill, G.; Gorman, C. B.; Tiemann, B. G.; Mansour, K. *Science* **1993**, *261*, 186–189.

(21) (a) Marcotte, N.; Fery-Forgues, S. *J. Chem. Soc., Perkin Trans. 2* **2000**, 1711–1716. (b) Detert, H.; Sugiono, E.; Kruse, G. *J. Phys. Org. Chem.* **2002**, *15*, 638–641. (c) Woo, H. Y.; Liu, B.; Kohler, B.; Korystov, D.; Mikhailovsky, A.; Bazan, G. C. *J. Am. Chem. Soc.* **2005**, *127*, 14721–14729. (d) Amthor, S.; Lambert, C.; Dümmler, S.; Fischer, I.; Schelter, J. *J. Phys. Chem. A* **2006**, *110*, 5204–5214. (e) Terenziani, F.; Painelli, A.; Katan, C.; Charlot, M.; Blanchard-Desce, M. *J. Am. Chem. Soc.* **2006**, *128*, 15742–15755.

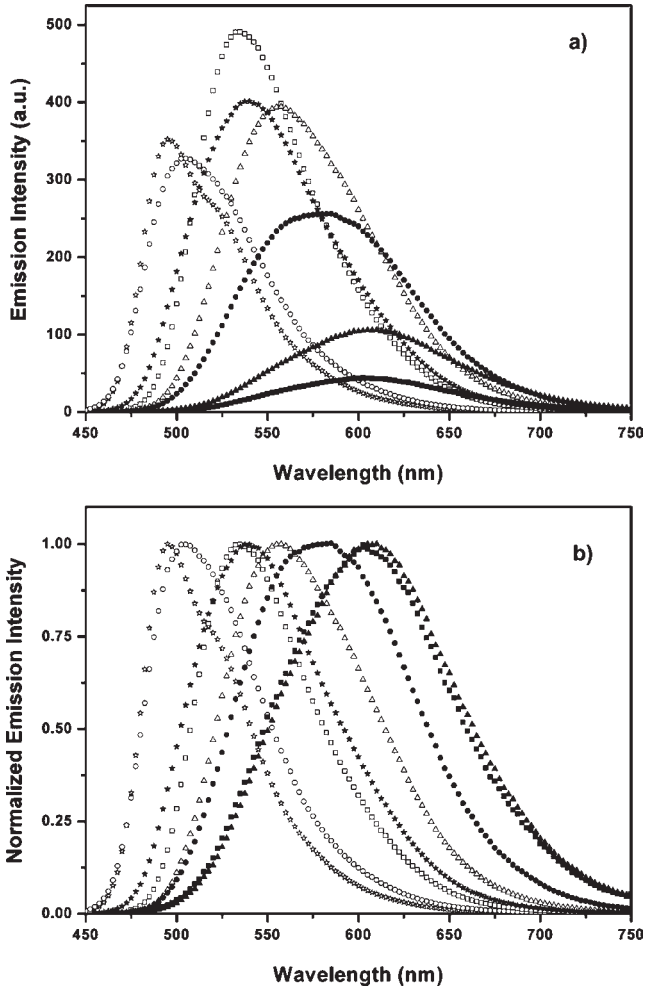

Figure 4. Fluorescence emission (a) absolute and (b) normalized spectra of **L** (1.0×10^{-6} M) in several solvents at 25 °C. Toluene (☆), diethylether (○), dichloromethane (△), chloroform (□), ethylacetate (★), 2-butanone (●), acetonitrile (▲), and ethanol (■).

Optical Spectroscopies. All optical measurements (i.e., absorption and emission spectra) have been performed in solution ($\sim 10^{-6}$ M) in a wide range of solvent polarity (from $\varepsilon = 1.88$ for *n*-hexane to $\varepsilon = 35.94$ for acetonitrile), and the results are summarized in Table 1 and Figures 3−4.

As shown in Figure 3, **L** exhibits a strong intense broad absorption band, which indicates a highly π-conjugated system. The spectral shape of the peak and the calculated molar absorption coefficient, ε_{max}, remained relatively constant ($\sim$ 70000 L mol^{-1} cm^{-1}) with solvent (Table 1). This absorption is attributed to a $\pi-\pi^*$ transition. As the solvent polarity increased, the absorption maxima were weakly red-shifted, up to 33 nm, ranging from 422 nm in *n*-hexane to 456 nm in ethanol.

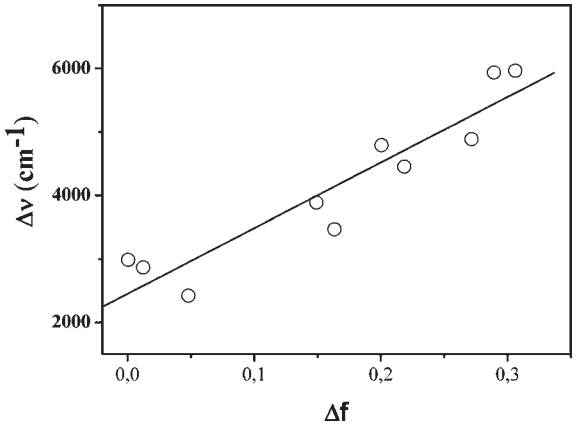

Figure 5. Plot of $\Delta\nu$ versus Δf, $[(\varepsilon-1)/(2\varepsilon+1) - (n^2-1)/(2n^2+1)]$ for **L** in different solvents.

While the absorption spectra of molecule **L** are only slightly solvent-dependent, it is obvious that the photoluminescence (PL) spectra show a pronounced bathochromic solvatochromism (Figure 4). Solution of **L** in *n*-hexane shows a fluorescence band exhibiting a well resolved vibrational structure with the maximum emission wavelength (λ_{em}) at 461 nm. When increasing solubility and solvent polarity a loss of the vibronic structure is observed, a progressive red-shift of the emission wavelength ($\lambda_{em} \sim$ 605 nm in acetonitrile) occurs, and the fluorescence quantum yield reaches a maximum and then decreases; the maximum value ($\phi_F = 0.97$) is obtained in chloroform.

Accordingly, the Stokes shifts ($\Delta\nu = \nu_{abs} - \nu_{em}$) significantly increase with increasing solvent polarity, ranging from 2438 cm^{-1} in triethylamine to 6045 cm^{-1} in acetonitrile. Such behavior, generally observed for dipolar compounds, indicates marked intramolecular charge transfer (ICT) in the excited state, inducing consequently a large dipole moment, stabilized in polar solvents. In the case of centrosymmetric quadrupolar molecules such as **L**, this behavior is attributed to symmetry breaking in the excited-state because of polar solvation.[21] The gain in the molecular dipole moments induced by the photoexcitation can be calculated by using the Lippert−Mataga relationship:[24−26]

$$\begin{aligned}\Delta\nu &= \nu_{\max}^{abs} - \nu_{\max}^{ems} \\ &= \frac{2(\mu_e-\mu_g)^2}{hca^3}\left(\frac{\varepsilon-1}{2\varepsilon+1} - \frac{n^2-1}{2n^2+1}\right) + Const. \\ &= \frac{2(\mu_e-\mu_g)^2}{hca^3}\Delta f + Const \end{aligned} \quad (1)$$

where μ_e and μ_g refer to the dipole moments of excited and ground states, respectively, h is Planck's constant, c is the velocity of light, a is the radius of the spherical Onsager

(22) (a) Laurence, C.; Nicolet, P.; Dalati, M. T.; Abboud, J.-L. M.; Notario., R. *J. Phys. Chem.* **1994**, *98*, 5807–5816. (b) McClellan., A. L. *Tables of Experimental Dipole Moments*; W. H. Freeman: San Francisco, 1963; Vol. *1*. (c) McClellan., A. L. *Tables of Experimental Dipole Moments*; Rahara Enterprises: El Cerrito, CA, 1974; Vol. *2*. (d) McClellan., A. L. *Tables of Experimental Dipole Moments*; Rahara Enterprises: El Cerrito, CA, 1986; Vol. *3*.

(23) (a) Marcus, Y. *J. Solution Chem.* **1991**, *20*, 929–944. (b) Reichardt, C. *Solvents and Solvent Effects in Organic Chemistry*, 2nd ed.; VCH: Weinheim, 1988; Chapter 7, p 339. (c) Reichardt, C. In *Solvents and Solvent Effects in Organic Chemistry*; VCH: Weinheim, Germany, 2004; Chapter 6−7.

(24) Lippert, E. *Z. Naturforsch. A* **1955**, *10*, 541–545.

(25) Mataga, N.; Kaifu, Y.; Koizumi, M. *Bull. Chem. Soc. Jpn.* **1956**, *29*, 465–470.

(26) Lippert, E.; Moll, F. Z. *Elektrochemie* **1954**, 718–724.

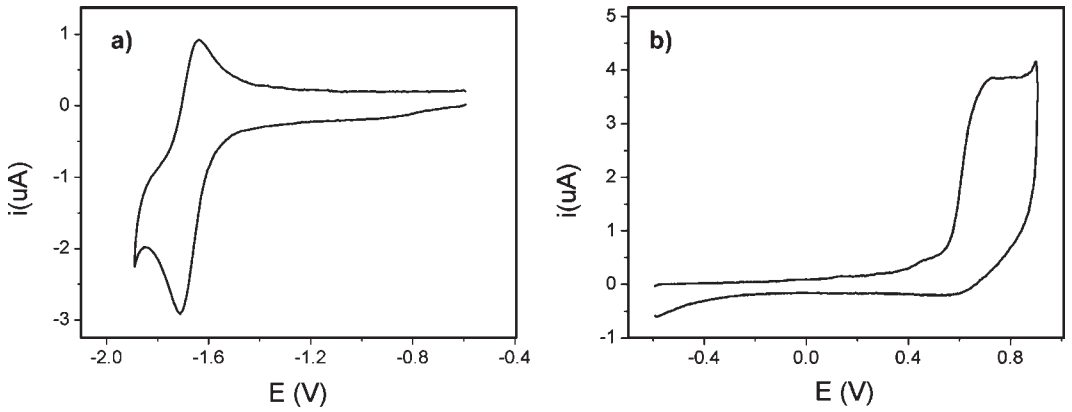

Figure 6. Cyclic voltammetry of **L** at a 1.1 mmol L^{-1} concentration in a toluene/acetonitrile mixture (50/50 v/v) containing 0.1 mol L^{-1} NBu_4BF_4 as a supporting electrolyte on a 1 mm diameter disk glassy carbon electrode: (a) reduction and (b) oxidation voltammograms. Scan rate = 0.2 s^{-1}; T = 20 °C, E in V versus SCE.

cavity[10b,c] which fits the molecule, and ε and n are the solvent dielectric constant and refractive index, and Δf is Lippert's function, respectively. As observed in Figure 5, a linear plot is obtained for compound **L**. On the basis of these data, the dipole moment difference between the ground and excited state, $\Delta\mu = \mu_\varepsilon - \mu_g$, could be calculated from the slope (10337 cm^{-1}) of the plot in Figure 5. A change of 19.3 D in dipole moment is deduced, using the Onsager's cavity radius (a_o) estimated as 7.18 Å by chemical modeling (see Experimental Section).[10b,c] Such a change confirms that the species formed in the excited state have different charge localization to that in the ground state, this result being consistent with a stabilization of highly polar emitting excited states by polar solvents.

Electrochemistry. In view of the potential application of compound **L** in optoelectronics, it is important to consider their respective energy gap $-\Delta E_g$, relative ionization potential (IP), and electron affinity (EA), parameters which characterize the facility for injecting holes and electrons, respectively, in the material. These values can be estimated from the first oxidation and reduction potentials in solution ($E_{ox}°$ and $E_{red}°$), which are associated to the HOMO and LUMO energy levels, respectively.[27] For this purpose, the electrochemical behavior of **L** was investigated by cyclic voltammetry (CV), to measure the redox potentials, and thus to estimate IP, EA, and the energy gap (that can be derived from their electrochemical gap $\Delta E_{g,elec} = E_{ox}° - E_{red}°$). Moreover, electrochemical measurements allow rapid determinations of the chemical stabilities (lifetimes) of the corresponding generated ionic species. The electrochemical oxidation and reduction of **L** were examined in toluene/acetonitrile mixture (50/50 v/v). This media allows a good solubility (in the millimolar range in most cases) of the studied compound as required for electrochemical experiments. Typical voltammograms of the reduction and oxidation of **L** are displayed in Figures 6 a and b respectively. In reduction (Figure 6a), **L** presents one well-defined reversible process. Considering that the reduction process was reversible at any investigated scan rate (down to 0.1 V s^{-1}), this results show a good chemical stability of the radical-anion (lifetime higher than 10 s) (Figure 6a).

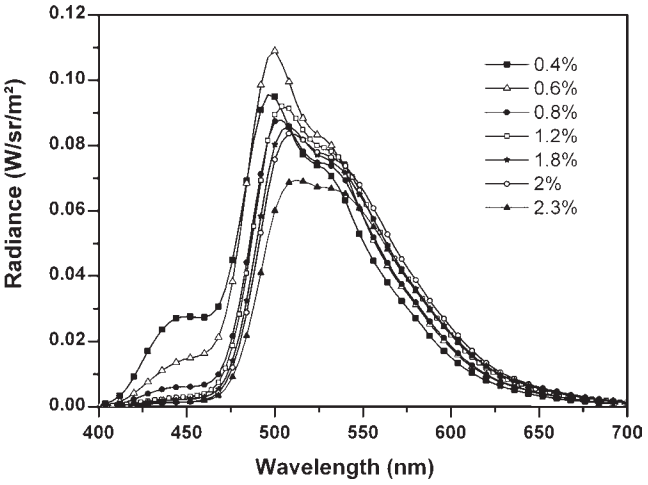

Figure 7. Electroluminescent spectra of the OLED at 30 mA cm^{-2} as a function of the percentage of dopant.

From this reversible voltammogram, the formal potential E^0_{red} was immediately derived as the half-sum between the forward and the reverse scan peak potentials (E^0_{red} = −1.68 V vs SCE). In oxidation, only one irreversible process was observed. This peak remains irreversible even when the scan rate was increased up to 100 V s^{-1} (Figure 6b), indicating that the lifetime of the produced radical cation is shorter than a few milliseconds in our experimental conditions. It is noticeable that the radical-cation has a much lower chemical stability than the corresponding radical-anion although in the presence of the two donating $N(Bu)_2$ groups. The $E°_{ox}$ value was approximated by the corresponding peak potential (E_{ox} = 0.69 V vs SCE), thus taking the previous $E°_{Red}$ values, leads to an electrochemical gap range about 2.37 eV. Concerning the HOMO and LUMO energy levels, to a first approximation, the oxidation potential can be related to the ionization potential and thus to the HOMO energy level, according to the following equation: HOMO = $(E_{ox} + 4.75)$.[27] The calculation shows that **L** possesses an ionization potential ranging in the 5.4 eV. A similar relationship can be made for the reduction potential, the electron affinity and LUMO energies, leading to an estimated high electron affinity (~3.1 eV). This value is higher than those previously determined on 6,6′-distyryl-3,

(27) Janietz, S.; Bradley, D. D. C.; Grell, M.; Giebeler, C.; Inbasekaran, M.; Woo, E. P. *Appl. Phys. Lett.* **1998**, *73*, 2453–2355.

Table 2. Electroluminescent Characteristics of the Devices Obtained at 30 mA cm^{-2} As a Function of the Doping Percentage

			efficiencies			CIE	
dopant in DPVBi (wt %)	λ_{em} (nm)	Us (V)	%	cd A^{-1}	lm W^{-1}	*x*	*y*
	452	5.3	3.6	4	1.2	0.155	0.130
0.4%	448/500/528	4.8	3.9	10.7	3.0	0.230	0.438
0.6%	450/500/527	5.3	4.1	12.1	3.2	0.245	0.503
0.8%	448/502/529	5.0	3.9	12.7	3.6	0.272	0.549
1.2%	504/529	5.1	4.2	13.7	3.6	0.285	0.570
1.8%	508/528	4.6	4	13.4	3.6	0.297	0.576
2%	508/529	5.3	4.1	14.1	3.7	0.306	0.583
2.3%	512/529	4.8	3.6	12.3	3.6	0.315	0.582

3′-bipyridine derivatives,[9a−c] and indicates that electrons could be easily injected in **L**.

Organic Light-Emitting Diode. The basic structure of the OLED device, presented in Figure 1 is ITO/CuPc/NPB/DPVBi: compound **L** (× wt %)/Alq_3/LiF/Al where × is the dopant ratio. The DPVBi is known to be a highly efficient blue emitter in multilayer OLED.[28] It has been used as well as an efficient matrix for white OLEDs with fluorescent dopant.[29] The compound **L** was selected to be tested in OLED because of a good fluorescent yield (70%) in solid (1% dispersion in PMMA thin film) in the green (emission at 528 nm). The percentage of dopant **L** was varied from 0.4% to 2.3% in DPVBi to determine its influence of the diode performances. The EL spectra of the devices are presented in Figure 7, and their electroluminescence (EL) performances and CIE coordinates are reported in Table 2. At low percentage of dopant (< 1%), the EL spectrum of the OLED comprises a small peak at 450 ± 4 nm, characteristic of the DPVBi emission and a peak around 505 nm with a shoulder at 528 nm, from the dopant emission. The small blue emission from DPVBi and the good quantum efficiencies (around 4%) of the doped devices evidence an efficient energy transfer from the host DPVBi to compound **L.** This energy transfer is likely favorable because of the energy levels of DPVBi and **L** (LUMO/HOMO of 2.8 eV/5.9 eV and 3.1 eV/4.75 eV respectively). Above 1% of dopant, the peak at 450 nm is negligible, and the emission comes only from **L**. The best performances at 30 mA cm^{-2} are obtained for the device at 2% of compound **L** and with a luminous efficiency of 14.1 cd A^{-1}, a power efficiency of 3.7 lm W^{-1} and an external quantum efficiency of 4.1%. The device emits green light with CIE coordinates $x = 0.306$ and $y = 0.583$. According to the device structure without enhanced light extraction system (Figure 1), an external quantum efficiency of 4% is close to the theoretical maximum value of 5% for OLEDs based on small fluorescent molecules like for the **L** material. The EL results show that DPVBi can be used as an efficient host for making green OLEDs.[30]

Complexations. To test the ability of compound **L** to form transition metal complexes, first the tetrahedral complex $[\mathbf{L_2Cu}]\mathbf{PF_6}$ and octahedral complex $[\mathbf{L_3Ni}](\mathbf{NO_3})_2$ (Chart 2) were synthesized. They were obtained in high yields upon dimethylformamide reflux treatment of free bipyridazine based ligand **L** with tetrakis(acetonitrile) copper(I) hexafluorophosphate (2:1) and nickel(II) nitrate hexahydrate (3:1), respectively. $[\mathbf{L_2Cu}]\mathbf{PF_6}$ and $[\mathbf{L_3Ni}](\mathbf{NO_3})_2$ FAB/Mass spectra are in accordance with the postulated structures of the Ni(II) and Cu(I) complexes.

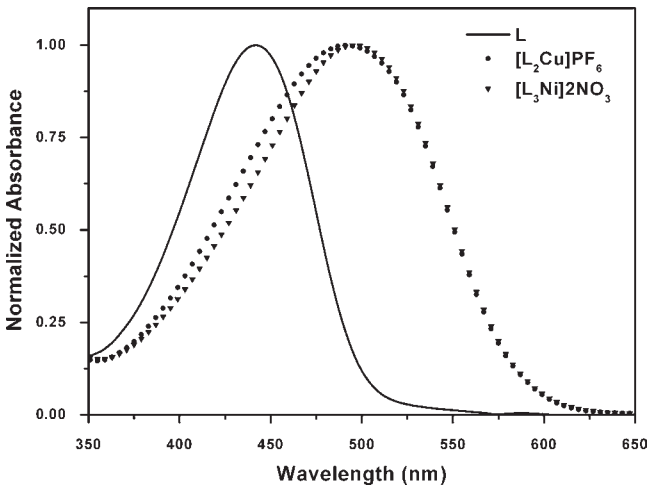

Figure 8. Normalized absorption spectra of the free bipyridazine based ligand **L** and related complexes $[\mathbf{L_2Cu}]\mathbf{PF_6}$ and $[\mathbf{L_3Ni}](\mathbf{NO_3})_2$ in acetone (1×10^{-5} mol L^{-1}) at 25 °C.

On the other hand, to reach other geometries, platinum (II) and iridium(III) complexes were as well routinely prepared from adequate metallic precursors such as $[Pt(DMSO)_2Cl_2]$, μ-di-Cl-$[Ir(C^N)_2Cl]_2$ (C^N account for orthometalated 2-phenylpyridine). Replacement of the chloro ligands by specific alkyne derivatives, in the $[\mathbf{LPtCl_2}]$ complex, was also promoted by copper(I) catalysis under anaerobic conditions. In the iridium complex a single isomer trans-(N) was isolated as unambiguously assigned by NMR spectroscopy.

Upon chelating with metal ions, linear optical properties are drastically changed as shown in Figures 8−11. Regarding the $[\mathbf{L_2Cu}]\mathbf{PF_6}$ and $[\mathbf{L_3Ni}](\mathbf{NO_3})_2$ complexes, an important red-shift of the intense ILCT (intraligand charge transfer) band is observed ($\Delta\lambda_{max} = 49$ and 55 nm, respectively, Figure 8) and no luminescence is observed in both cases.

On the other hand, upon chelating of Pt or Ir centers, complexes exhibit completely different optical spectra as shown in Figures 9−11. First, the yellow color of the free ligand is replaced by an intense blue and dark violet color, respectively, complexation of ligand **L** with Pt inducing a bathochromic shift of the lowest absorption to 608 nm. This absorption is likely assigned to a MLCT as previously

(28) Shaheen, S. E.; Jabbour, G. E.; Morrell, M. M.; Kawabe, Y.; Kippelen, B.; Peyghambarian, N.; Nabor, M.-F.; Schlaf, R.; Mash, E. A.; Armstrong, N. R. *J. Appl. Phys.* **1998**, *84*, 2324–2327.

(29) Geffroy, B.; Lemaitre, N.; Lavigne, J.; Denis, C.; Maisse, P.; Raimond, P. *Nonlinear Opt., Quantum Opt.* **2007**, *37*, 9–19.

(30) (a) Tang, C. W.; VanSlycke, S. A.; Chen, C. H. *J. Appl. Phys.* **1989**, *65*, 3610. (b) Liu, T. H.; Iou, C. Y.; Wen, S. W.; Chen, C. H. *Thin Solid Films* **2003**, *441*, 223–227.

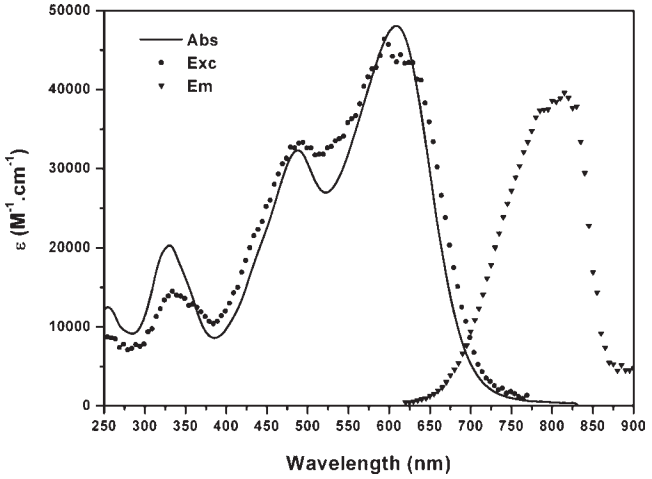

Figure 9. Absorption (1×10^{-5} M), emission (2×10^{-6} M, $\lambda_{ex} = 550$ nm) and excitation spectra ($\lambda_{em} = 826$ nm) of **[LPtCl$_2$]** in dichloromethane at 25 °C.

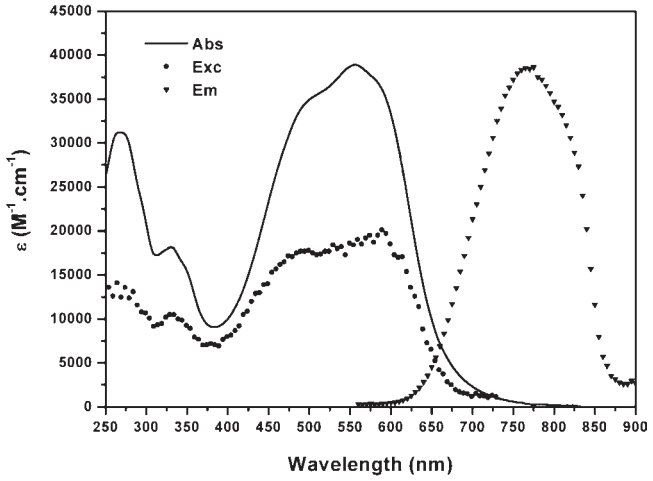

Figure 10. Absorption (1×10^{-5} M), emission (1×10^{-6} M, $\lambda_{ex} = 550$ nm) and excitation spectra ($\lambda_{em} = 776$ nm) of **[LPt(-≡-Ph)$_2$]** in dichloromethane at 25 °C.

observed for related derivatives.[31] Interestingly, by substitution of the two chloro ligands by tolylacetylene residues such as in the Pt-≡- case, the less energetic absorption is an envelope including at least two major absorptions safely assigned to a MLCT and a LLCT band clearly observed on the red side of the band (Figure 9),[32] this latter band being absent in the corresponding **[LPtCl$_2$]** complex. Clearly the signature of the tolylacetylene fragments is also found in the intense $\pi-\pi^*$ absorption at 267 nm which is absent in the precursor absorption spectra. Second, both platinum complexes are weakly emissive in the near IR regime at 744 and 766 nm (Figures 9 and 10). In both cases the positions of the absorption bands is not dependent on the concentration in the 10^{-5} to 10^{-7} M range which exclude metal−metal aggregation or strong $\pi-\pi$ interactions. For **[LPt(-≡-Ph)$_2$]** the emission quantum yield is 0.19 in

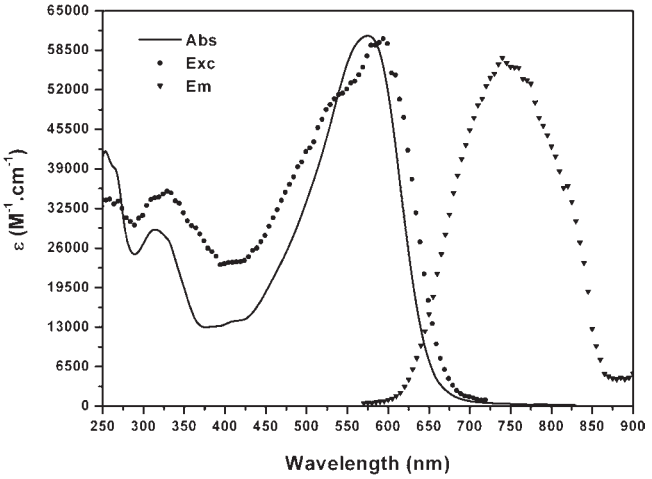

Figure 11. Absorption (1×10^{-5} M), emission (2×10^{-6} M, $\lambda_{ex} = 550$ nm) and excitation ($\lambda_{em} = 754$ nm) spectra of **[LIr(C^N)$_2$]BF$_4$** in dichloromethane at 25 °C.

degassed conditions and falls to 0.08 in air. Clearly, the oxygen dependence of the quantum yield is in favor of phosphorescence from a MLCT excited state. For the **[LPtCl$_2$]** complex the emission quantum yield is too weak to be measured precisely. Unfortunately, we were unable to measure accurately the lifetime of the platinum complexes with our experimental setup because of the weak emission intensity. However, in both platinum complexes the excitation spectrum reveals a perfect match with the absorption spectra which is a proof for the contribution of all absorption in the luminescence of the complexes (Figures 9 and 10).

The Ir complex reveals similar bathochromic shifts and a strong absorption at 608 nm which is also attributed to a dual absorption of the MLCT and ligand centered (LC) transitions.[33] In this case an emission quantum yield of 0.36 was determined at 816 nm whereas this yield drops to 0.08 in non-degassed conditions. The excitation spectrum overlaps the absorption spectra (Figure 11). For the **[LIr(C^N)$_2$]$^+$** complex an excited state lifetime of 190 ± 35 ns has been determined which is in favor for a phosphorescence from an MLCT manifold as previously found for related Ir-complexes.[33] For all three complexes the same generic spectral features are retained in dichloromethane in which the Beer−Lambert law is followed. Further characterization of these excited states is currently in progress and falls outside of the scope of this contribution.

In addition, the electrochemical data of these complexes are summarized in Table 3. All the complexes show one irreversible oxidation peak around +0.76/+0.79 V versus SCE likely because of the irreversible oxidation of the dibutylamino residues of ligand **L** (found at +0.70 V vs SCE in dichloromethane). For the Ir complex an additional quasi reversible oxidation process was found at +1.32 V in keeping with the oxidation of the Ir center as found in related complexes.[34]

For each complex two reversible reduction processes were found at a potential less cathodic versus the free

(31) Shikhova, E.; Danilov, E. O.; Kinayyigit, S.; Pomestchenko, I. E.; Tregubov, A. D.; Camerel, F.; Retailleau, P.; Ziessel, R.; Castellano, F. N. *Inorg. Chem.* **1997**, *36*, 3038–3048.
(32) Clark, M. L.; Diring, S.; Retailleau, P.; McMillin, D. R.; Ziessel, R. *Chem.—Eur. J.* **2008**, *14*, 7168–7179.
(33) Colombo, M. G.; Hauser, A.; Güdel, H. U. *Top. Curr. Chem.* **1994**, *171*, 143–171.
(34) Lowry, M. S.; Bernhard, S. *Chem.—Eur. J.* **2006**, *12*, 7970–7977.

Table 3. Cyclic Voltammetry Data at 20 °C[a]

	E_{ap} (ox, soln) (V), ΔE (mV)	$E^{0'}$(red, soln) (V), ΔE (mV)
$[LPtCl_2]$	+0.76 (irr.)	−0.87 (60), −1.46 (70)
$[LPt(-\equiv-Ph)_2]$	+0.79 (irr.)	−1.00 (70), −1.57 (80)
$[LIr(C^\wedge N)_2]BF_4$	+0.77 (irr.) +1.32 (90)	−1.12 (60), −1.68 (80)

[a] Potentials determined by cyclic voltammetry in anhydrous and deoxygenated CH_2Cl_2 solution, containing 0.1 M $TBAPF_6$, [electrochemical window from +1.6 to −2.2 V], at a solute concentration of about 1.0 mM, using a scan rate of 200 mV s^{-1} unless otherwise indicated. Potentials were standardized versus ferrocene (Fc) as internal reference and converted to the SCE scale assuming that $E_{1/2}$ (Fc/Fc^+) = +0.38 V (ΔEp = 60 mV) versus SCE. For reversible processes $E_{1/2}$ = (E_{pa} + E_{pc})/2. Error in half-wave potentials is ±10 mV. For irreversible processes the peak potentials (E_{ap}) are quoted. All reversible redox steps result from one-electron processes except otherwise quoted.

ligand **L** when studied under the same conditions (−1.66 V vs SCE). The redox wave separation is 590, 570, and 560 mV for **[LPtCl$_2$]**, **[LPt(-≡-Ph)$_2$]**, and **[LIr(C^N)$_2$]$^+$**, respectively. For the Pt complexes the relative insensitivity of the reduction potentials toward the nature of the acetylide or chloro ligand suggests that these reductions are mainly localized on the ligand **L** with some mixing with the Pt(II) metal orbitals.[35,36] These data are consistent with data found with related $[Pt(^tBu_3tpy)X]^+$ complexes.[37]

The cyclic voltammetry data for the Ir complex is in keeping with related orthometalated complexes where the reduction occurs at a more negative potential versus the Pt complexes. Likewise the first reduction is likely assigned to the reduction of the coordinated ligand **L** whereas the second reduction is attributed to the orthometalated C^N ligand in light of redox properties determined in related complexes.[38]

Conclusions

We succeeded in the preparation of a new π-conjugated 3,3′-bipyridazine ligand carrying two dibutylamino donor groups. This yellow and highly fluorescent compound (green emitter) exhibits a pronounced intramolecular charge transfer excited state of push−pull type, the acceptor being represented by the central 3,3′-bipyridazine core. The compound is subjected to a pronounced solvatochromism which has been studied in some detail. Its emission properties were exploited to build an organic light emitting device (OLED) by doping into a fluorescent DPVBi matrix. The best device provides a power efficiency of 3.7 lm W^{-1} and an external efficiency of 4.1% with a doping ratio of 2% of **L** into DPVBi. Complexation of the ligand with Cu(I) or Ni(II) salts provide respectively tetrahedral and octahedral geometries in which the fluorescence of the ligand is quenched. Complexation of ligand **L** to square planar Pt(II) or octahedral Ir(III) complexes is also feasible providing robust complexes weakly luminescent in the near-infrared. The rich electroactivity of these latter complexes is due to the presence of surrounding ligands (σ-ethynyl moieties for Pt and orthometalated C^N framents for Ir). The versatility of the chemistry disclosed here opens interesting perspectives for modifications of the donor/acceptor character of the terminal substituents of the molecule and consequently for the tuning of the electronic properties. The solvatochromism in emission and fluorescence quenching upon complexation with the first series of transition metals would also be auspicious for the design of integrated chemical sensors. In the same way, the design of new ligands and the application of them in the synthesis of heavy-metal complexes to obtain phosphorescent emitters (e.g., ruthenium complexes) as sensitizers are currently in progress.

Acknowledgment. We gratefully acknowledge helpful technical support for mass spectrometry from Pr. Lange and from Pr. Rammondec, both from the IRCOF Institute (Rouen); many thanks are due as well to Pr. Le Bozec from O2's Group (Rennes University) for very fruitful scientific discussion and help concerning complexation aspects. Dr. Stéphane Diring is acknowledged for the first synthesis of a small sample of the platinum complexes. Raymond Ziessel (Strasbourg) warmly thanks Johnson Matthey PLC for a loan of precious metal salts.

Note Added after ASAP Publication. An acknowledgment sentence was added along with several other text changes throughout this paper which was published ASAP April 2, 2010; the version containing the changes reposted on April 9, 2010.

(35) Hill, M. G.; Bailey, J. A.; Miskowski, V. M.; Gray, H. B. *Inorg. Chem.* **1996**, *35*, 4585–4590.
(36) Crites, D. K.; Cunningham, C. T.; McMillin, D. R. *Inorg. Chim. Acta* **1998**, *273*, 346–353.
(37) Rachford, A. A.; Goeb, S.; Ziessel, R.; Castellano, F. N. *Inorg. Chem.* **2008**, *47*, 4348–4355.
(38) Slinker, J. D.; Gorodetsky, A. A.; Lowry, M. S.; Wang, J.; Parker, S.; Rohl, R.; Berhard, S.; Malliaras, G. G. *J. Am. Chem. Soc.* **2004**, *126*, 2763–2767.